

1 **Favipiravir antiviral efficacy against SARS-CoV-2 in a hamster model**

2 Jean-Sélim Driouich^{1#}, Maxime Cochin^{1#}, Guillaume Lingas², Grégory Moureau¹, Franck Touret¹, Paul
3 Rémi Petit¹, Géraldine Piorkowski¹, Karine Barthélémy¹, Bruno Coutard¹, Jérémie Guedj², Xavier de
4 Lamballerie¹, Caroline Solas^{1,3}, Antoine Nougairède^{1*}

5 ¹: Unité des Virus Émergents, UVE: Aix Marseille Univ, IRD 190, INSERM 1207, Marseille, France.

6 ²: Université de Paris, IAME, INSERM, F-75018 Paris, France

7 ³: Laboratoire de Pharmacocinétique et Toxicologie, Hôpital La Timone, APHM, Marseille, France

8 [#]Contributed equally

9 *Corresponding author: antoine.nougairede@univ-amu.fr

10 **Abstract**

11 Despite no or limited pre-clinical evidence, repurposed drugs are massively evaluated in clinical trials
12 to palliate the lack of antiviral molecules against SARS-CoV-2. Here we used a Syrian hamster model to
13 assess the antiviral efficacy of favipiravir, understand its mechanism of action and determine its
14 pharmacokinetics. When treatment was initiated before or simultaneously to infection, favipiravir had
15 a strong dose effect, leading to dramatic reduction of infectious titers in lungs and clinical alleviation
16 of the disease. Antiviral effect of favipiravir correlated with incorporation of a large number of
17 mutations into viral genomes and decrease of viral infectivity. The antiviral efficacy observed in this
18 study was achieved with plasma drug exposure comparable with those previously found during human
19 clinical trials and was associated with weight losses in animals. Thereby, pharmacokinetic and
20 tolerance studies are required to determine whether similar effects can be safely achieved in humans.

21 **Keywords**

22 COVID-19, SARS-CoV-2, antiviral therapy, favipiravir, animal model, preclinical research

23 Introduction

24 In March 2020, the World Health Organization declared coronavirus disease 2019 (COVID-19) a
25 pandemic¹. The COVID-19 outbreak was originally identified in Wuhan, China, in December 2019 and
26 spread rapidly around the world within a few months. The severe acute respiratory syndrome
27 coronavirus 2 (SARS-CoV-2), the causative agent of COVID-19, belongs to the *Coronaviridae* family and
28 is closely related to the SARS-CoV which emerged in China in 2002². After an incubation period of about
29 5 days, disease onset usually begins with an influenza-like syndrome associated with high virus
30 replication in respiratory tracts^{3,4}. In some patients, a late acute respiratory distress syndrome,
31 associated with high levels of inflammatory proteins, occurs within one to two weeks³. As of 7 July
32 2020, more than 11.6 million cases of COVID-19 have resulted in more than 538,000 deaths⁵. In the
33 face of this ongoing pandemic and its unprecedented repercussions, not only on human health but
34 also on society, ecology and economy, there is an urgent need for effective infection prevention and
35 control measures.

36 Whilst host-directed and immune-based therapies could prove useful for the clinical management of
37 critically ill patients, the availability of safe and effective antiviral molecules would represent an
38 important step towards fighting the current pandemic. As conventional drug development is a slow
39 process, repurposing of drugs already approved for any indication was extensively explored and led to
40 the implementation of many clinical trials for the treatment of COVID-19⁶. However, the development
41 of effective antiviral drugs for the treatment of COVID-19, should, as much as possible, rely on robust
42 pre-clinical *in vivo* data, not only on efficacy generated *in vitro*. Accordingly, rapid implementation of
43 rodent and non-human primate animal models should help to assess more finely the potential safety
44 and efficacy of drug candidates and to determine appropriated dose regimens in humans^{7,8}.

45 Favipiravir (6-fluoro-3-hydroxypyrazine-2-carboxamine) is an anti-influenza drug approved in Japan
46 that has shown broad-spectrum antiviral activity against a variety of other RNA viruses⁹⁻¹⁵. Favipiravir
47 is a prodrug that is metabolized intracellularly into its active ribonucleoside 5'-triphosphate form that
48 acts as a nucleotide analogue to selectively inhibit RNA-dependent RNA polymerase and induce lethal
49 mutagenesis^{16,17}. Recently, several studies reported *in vitro* inhibitory activity of favipiravir against
50 SARS-CoV-2 with 50% effective concentrations (EC₅₀) ranging from 62 to >500μM (10 to >78μg/mL)¹⁸⁻
51 ²⁰. Based on these results, more than 20 clinical trials on the management of COVID-19 by favipiravir
52 are ongoing (<https://clinicaltrials.gov/>). In the present study, a Syrian hamster model (*Mesocricetus*
53 *auratus*) was implemented to explore the *in vivo* safety and efficacy and the pharmacokinetics (PK) of
54 several dosing regimens of favipiravir.

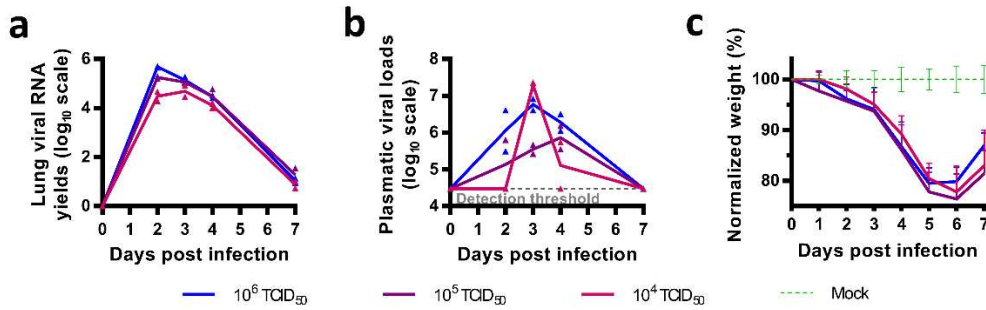
55 **Results**

56 ***In vitro* efficacy of favipiravir**

57 Using VeroE6 cells and an antiviral assay based on reduction of cytopathic effect (CPE), we recorded
58 EC₅₀ and EC₉₀ of 32 and 52.5 µg/mL using a multiplicity of infection (MOI) of 0.001, 70.0 and >78.5µg/mL
59 with an MOI of 0.01 (Figure S1) in accordance with previous studies¹⁸⁻²⁰. Infectious titer reductions
60 (fold change in comparison with untreated cells) were ≥2 with 19.6µg/mL of favipiravir and ranged
61 between 11 and 342 with 78.5µg/mL. Using CaCo2 cells, which do not exhibit CPE with SARS-CoV-2
62 BavPat1 strain, infectious titer reductions were around 5 with 19.6µg/mL of favipiravir and ranged
63 between 144 and 7721 with 78.5µg/mL of the drug. 50% cytotoxic concentrations (CC₅₀) in VeroE6 and
64 CaCo2 cells were >78.5µg/mL.

65 **Infection of Syrian hamsters with SARS-CoV-2**

66 Following Chan *et al.*, we implemented a hamster model to study the efficacy of antiviral compounds⁷.
67 Firstly, we intranasally infected four-week-old female Syrian hamsters with 10⁶ TCID₅₀ of virus. Groups
68 of two animals were sacrificed 2, 3, 4 and 7 days post-infection (dpi). Viral replication was quantified
69 in sacrificed animals by RT-qPCR in organs (lungs, brain, liver, small/large bowel, kidney, spleen and
70 heart) and plasma. Viral loads in lungs peaked at 2 dpi, remained elevated until 4 dpi and dramatically
71 decreased at 7 dpi (Figure 1a). Viral loads in plasma peaked at 3 dpi and viral replication was detected
72 in the large bowel at 2 dpi (Figure 1b and Table S1). No viral RNA was detected in almost all the other
73 samples tested (Table S1). Subsequently, we infected animals with two lower doses of virus (10⁵ and
74 10⁴ TCID₅₀). Viral RNA was quantified in lungs, large bowel and plasma from sacrificed animals 2, 3, 4
75 and 7 dpi (Figure 1a and 1b). Viral loads in lungs peaked at 2 and 3 dpi with doses of 10⁵ and 10⁴ TCID₅₀
76 respectively. Maximum viral loads in lungs of animals infected with each dose of virus were
77 comparable. Viral RNA yields in plasma and large bowel followed a similar trend but with more
78 variability, with this two lower doses. In addition, clinical monitoring of animals showed no marked
79 symptoms of infection but significant weight losses from 3 dpi when compared to animals intranasally
80 inoculated with sodium chloride 0.9% (Figure 1c).



81
82 **Figure 1: Implementation of hamster model**

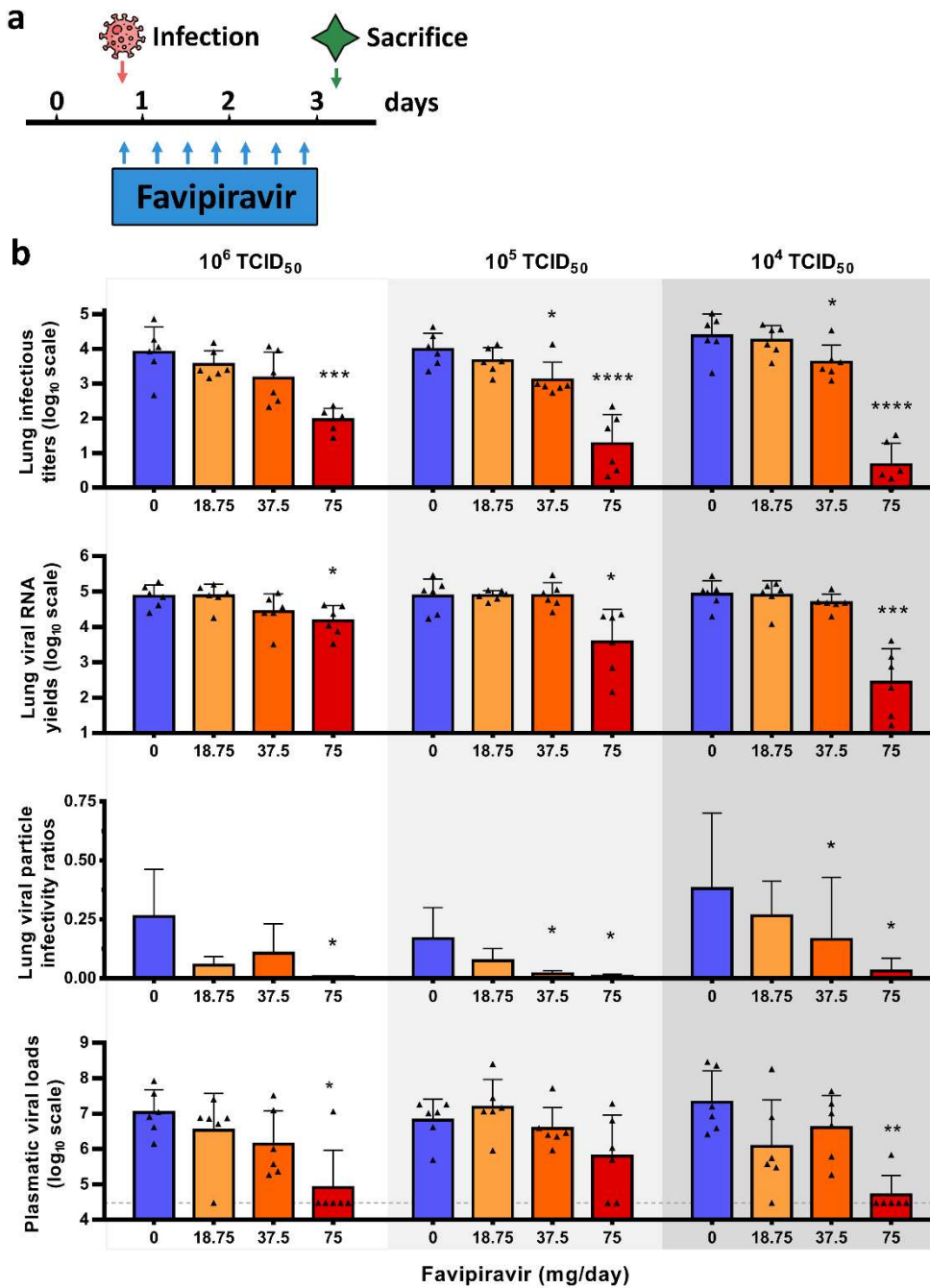
83 Hamsters were intranasally infected with 10⁶, 10⁵ or 10⁴ TCID₅₀ of virus. Viral replication was quantified using
84 an RT-qPCR assay. **a** Lung viral RNA yields. **b** Plasmatic viral loads. **c** Clinical course of the disease. Normalized
85 weight at day *n* was calculated as follows: (% of initial weight of the animal at day *n*)/(mean % of initial weight
86 for mock-infected animals at day *n*). Data represent mean \pm SD (details in Table S1).

87 *In vivo* efficacy of favipiravir

88 To assess the efficacy of favipiravir, hamsters received the drug, intraperitoneally, three times a day
89 (TID). We used three doses of favipiravir: 18.75, 37.5 and 75mg/day (corresponding to 340 \pm 36, 670 \pm 42
90 and 1390 \pm 126 mg/kg/day respectively).

91 In a first set of experiments, treatment was initiated at day of infection (preemptive antiviral therapy)
92 and ended at 2 dpi. We infected groups of 6 animals intranasally with three doses of virus (10⁶, 10⁵ and
93 10⁴ TCID₅₀) and viral replication was measured in lungs and plasma at 3 dpi (Figure 2a). When analysis
94 of virus replication in clarified lung homogenates was based on infectious titers (as measured using
95 TCID₅₀ assay), the effect of favipiravir in reducing infectious titers was dose dependent, in particular
96 when low doses of virus were used to infect animals (Figure 2b). At each dose of virus, mean infectious
97 titers for groups of animals treated with 75mg/day TID were significantly lower than those observed
98 with untreated groups ($p\leq 0.0001$): reduction of infectious titers ranged between 1.9 and 3.7 log₁₀. For
99 animals infected with 10⁵ or 10⁴ TCID₅₀, significant infectious titer reductions of around 0.8 log₁₀ were
100 also observed with the dose of 37.5mg/day TID ($p\leq 0.038$). Drug 90% and 99% effective doses (ED₉₀ and
101 ED₉₉) were estimated based on these results and ranged between 31-42mg/day and 53-70mg/day
102 respectively (Table 2). When analysis of virus replication in clarified lung homogenates were assessed
103 on viral RNA yields (as measured using quantitative real time RT-PCR assay), significant differences
104 with groups of untreated animals, ranging between 0.7 and 2.5 log₁₀, were observed only with the
105 higher dose of favipiravir ($p\leq 0.012$). Once again, this difference was more noticeable with lower doses
106 of virus (Figure 2b). Since we found higher reductions of infectious titers than those observed with viral
107 RNA yields, we estimated the relative infectivity of viral particle (*i.e.* the ratio of the number of
108 infectious particles over the number of viral RNA molecules). Decreased infectivity was observed in all
109 treated groups of animals. These differences were always significant with the higher dose of favipiravir

110 ($p \leq 0.031$) and were significant with the dose of 37.5mg/day TID for animals infected with 10^5 or 10^4
111 TCID₅₀ of virus ($p \leq 0.041$). We then measured plasmatic viral loads using quantitative real time RT-PCR
112 assay and found, with the higher dose of favipiravir and the groups of animals infected with 10^6 or 10^4
113 TCID₅₀, significant reductions of 2.1 and 2.62 log₁₀, respectively ($p \leq 0.022$) (Figure 2b).



114

115 **Figure 2: Virological results with preemptive favipiravir therapy**

116 a Experimental timeline. b Virological results with preemptive favipiravir therapy. Hamsters were intranasally infected with 10⁶,
117 10⁵ or 10⁴ TCID₅₀ of virus. Lung infectious titers (measured using a TCID₅₀ assay) and viral RNA yields were
118 (measured using an RT-qPCR assay) expressed in TCID₅₀/copy of -actine gene and viral genome copies/copy of
119 -actine gene respectively. Relative lung viral particle infectivities were calculated as follows: ratio of lung

120 infectious titer over viral RNA yields. Plasmatic viral loads (measured using an RT-qPCR assay) are expressed in
121 viral genome copies/mL of plasma (the dotted line indicates the detection threshold of the assay). Data represent
122 mean \pm SD. ****, ***, ** and * symbols indicate that the average value for the group is significantly lower than
123 that of the untreated group with a p-value <0.0001, ranging between 0.0001-0.001, 0.001-0.01 and 0.01-0.05
124 respectively (details in Table S2 and S3).

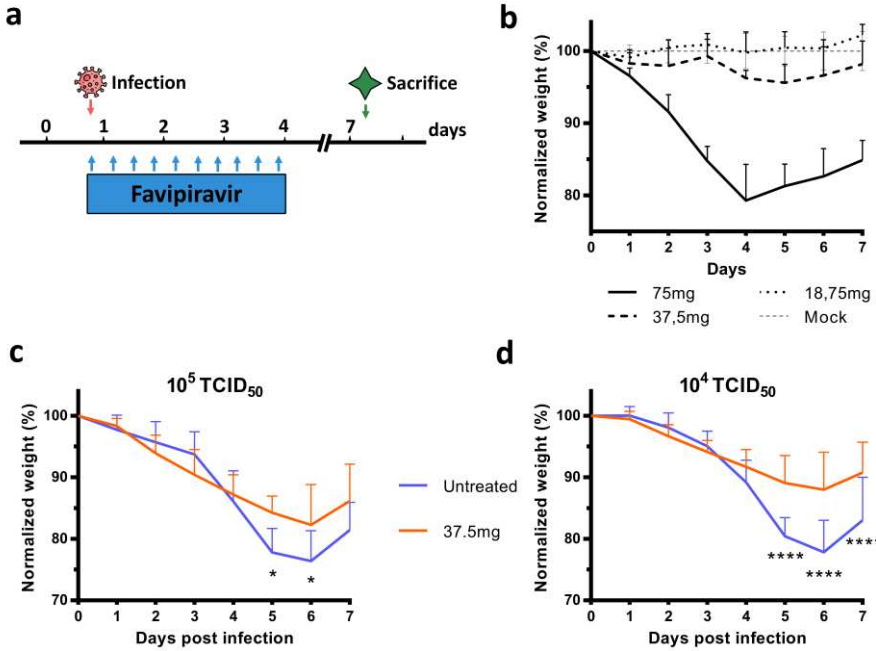
125 **Table 2: Drug effective doses (ED) on reducing viral titers according to the level of viral inoculum**

	ED ₅₀ mg/day (95%CI ¹)	ED ₉₀ mg/day (95%CI ¹)	ED ₉₉ mg/day (95%CI ¹)
Preemptive therapy			
10 ⁴ TCID ₅₀	34 (30-37)	42 (38-46)	53 (48-58)
10 ⁵ TCID ₅₀	26 (21-30)	37 (31-44)	56 (46-65)
10 ⁶ TCID ₅₀	15 (10-20)	31 (21-41)	70 (48-93)
Preventive therapy			
10 ⁴ TCID ₅₀	27 (25-29)	35 (32-38)	47 (44-51)

¹: 95% confidence interval

Dose-response curves are presented in Figure S2.

126 In a second set of experiments, we assessed, over a period of 7 days, the impact of treatment on the
127 clinical course of the disease using weight loss as the primary criterion (Figure 3a). Beforehand, we
128 evaluated the toxicity of the three doses of favipiravir with groups of four non-infected animals treated
129 from day 0 to day 3 (Figure 3b). High toxicity was observed with the dose of 75mg/day TID with
130 significant weight loss noticed from the first day of treatment (Table S4). We also found a constant,
131 but moderate, toxicity with the dose of 37.5mg/day TID that was significant at day 4 and 5 only. No
132 toxicity was detected with the lower dose of favipiravir. To assess if the toxicity observed with the
133 highest dose of favipiravir was exacerbated by the infection, we compared weight losses of infected
134 and non-infected animals treated with the dose of 75mg/day TID. Regardless of the dose of virus, no
135 significant difference was observed at 1, 2 and 3 dpi (Figure S3). After this evaluation of favipiravir
136 toxicity, we intranasally infected groups of 10 animals with two doses of virus (10⁵ or 10⁴ TCID₅₀).
137 Treatment with a dose of 37.5mg/day TID was initiated on the day of infection (preemptive antiviral
138 therapy) and ended at 3 dpi (Figure 3a). With both doses of virus, treatment was associated with
139 clinical alleviation of the disease (Figure 3c-d). With the dose of 10⁵ TCID₅₀, mean weights of treated
140 animals were significantly higher than those of untreated animals at 5 and 6 dpi ($p \leq 0.031$). Similar
141 observations were made with the dose of 10⁴ TCID₅₀ at 5, 6 and 7 dpi ($p < 0.0001$).

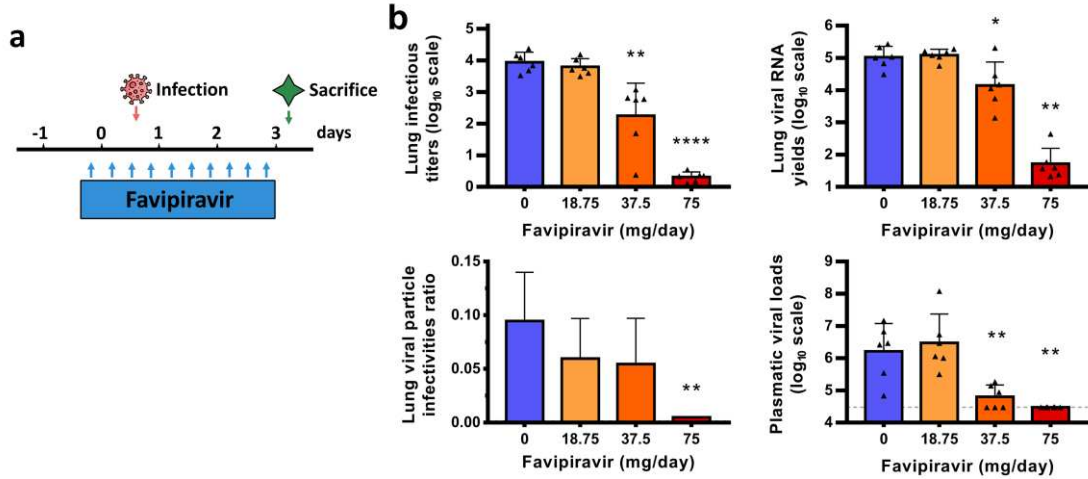


142

143 **Figure 3: Clinical follow-up of animals**

144 **a** Experimental timeline. **b** Evaluation of the toxicity of the three doses of favipiravir (mg/day TID) with uninfected
145 animals following an identical experimental timeline without infection. **c-d** Clinical follow-up with animals
146 infected respectively with 10^5 and 10^4 TCID₅₀ of virus and treated with a dose of favipiravir of 37.5mg/day TID.
147 Normalized weight at day n was calculated as follows: (% of initial weight of the animal at day n)/(mean % of
148 initial weight for mock-infected animals at day n). Data represent mean \pm SD. **** and * symbols indicate a
149 significant difference between treated and untreated animals with a p-value <0.0001 and ranging between 0.01-
150 0.05 respectively (details in Table S2 and S4).

151 In a third set of experiments, treatment was started one day before infection (preventive antiviral
152 therapy) and ended at 2 dpi. We intranasally infected groups of 6 animals with 10^4 TCID₅₀ of virus and
153 viral replication was measured in lungs and plasma at 3 dpi (Figure 4a). Once again, an inverse
154 relationship was observed between lung infectious titers and the dose of favipiravir (Figure 4b). Mean
155 infectious titers for groups of animals treated with 37.5 and 75mg/day TID were significantly lower
156 than those observed with untreated groups ($p \leq 0.002$). Of note, undetectable infectious titers were
157 found for all animals treated with the higher dose. Estimated ED₉₀ and ED₉₉ were 35 and 47mg/day
158 respectively (Table 2). Significant reductions of viral RNA yields of 0.9 and 3.3 log₁₀, were observed with
159 animals treated with 37.5 and 75mg/day TID respectively ($p \leq 0.023$). Resulting infectivity of viral
160 particle was decreased, with a significant reduction only for the higher dose of favipiravir ($p=0.005$).
161 Finally, we found significantly reduced plasmatic viral loads with animals treated with 37.5 and
162 75mg/day TID ($p \leq 0.005$).



163

164 **Figure 4: Virological results with preventive favipiravir therapy**

165 **a** Experimental timeline. **b** Viral replication in lungs and plasma. Hamsters were intranasally infected with 10^4
166 TCID₅₀ of virus. Lung infectious titers (measured using a TCID₅₀ assay) and viral RNA yields (measured
167 using an RT-qPCR assay) are expressed in TCID₅₀/copy of β -actine gene and viral genome copies/copy of
168 β -actine gene respectively. Relative lung virus infectivities were calculated as follows: ratio of lung infectious titer
169 over viral RNA yields. Plasmatic viral loads (measured using an RT-qPCR assay) are expressed in viral genome
170 copies/mL of plasma (the dotted line indicates the detection threshold of the assay). Data represent mean \pm SD.
171 *** and ** symbols indicate that the average value for the group is significantly different from that of the
172 untreated group with a p-value <0.0001 , ranging between 0.001-0.01 and 0.01-0.05 respectively (details in Table
173 S2 and S3).

174 **Favipiravir pharmacokinetics (PK) in a hamster model**

175 We first assessed the PK and lung distribution of favipiravir in a subgroup of uninfected animals. Groups
176 of animals were treated respectively with a single dose of favipiravir administrated intraperitoneally:
177 6.25mg, 12.5mg and 25mg. In each dose group, we sacrificed 3 animals at specific time points post-
178 treatment (0.5, 1, 5 or 8 hours) for determination of favipiravir in plasma. Drug concentration in lung
179 tissue was determined at 0.5 and 5 hours post-treatment. Subsequently, we assessed the favipiravir
180 concentration after multiple dose in animals intranasally infected with 10^5 TCID₅₀ of virus. Groups of 9
181 animals received the three doses evaluated for 3 days (Figure 2a): 18.75mg/day, 37.5mg/day and
182 75mg/day TID and were sacrificed at 12-hours after the last treatment dose. Favipiravir was quantified
183 in plasma (n=9) and lung tissue (n=3).

184 Results are presented in Table 3 and Figure S4. The single dose PK analysis showed that the maximum
185 concentration of favipiravir was observed at 0.5 hour at all doses, then plasma drug concentrations
186 decreased exponentially to reach concentrations below 10 μ g/ml at 12 hours. Favipiravir PK exhibited
187 a non-linear increase in concentration between the doses. After multiple doses, trough concentrations
188 (12 hours) of favipiravir also exhibited a non-linear increase between doses. The extrapolated 12 hours
189 post-treatment concentrations after a single dose were calculated in order to determine the

190 accumulation ratio. Accumulation ratios were respectively 6, 16 and 21 at the 3 doses, confirming the
191 non-proportional increase between doses. The average concentration after single dose administration
192 over 0 to 12-hour intervals was calculated and the respective values obtained were 10.1 μ g/mL,
193 38.7 μ g/mL and 100.5 μ g/mL for the 3 favipiravir doses.

194 Favipiravir lung concentrations were 1.6 to 2.7-fold lower than in plasma for both administration of
195 single and multiple doses. After a single dose, the mean lung to plasma ratio ranged from 0.37 to 0.62
196 according to the time post-treatment and was similar between the 3 doses of favipiravir at 0.5 hours.
197 A high ratio 5 hours post-treatment was observed at the highest dose (25mg) with an increase by a
198 factor 1.6 to 1.8 compared with the lower doses. After multiple doses, the lung penetration of
199 favipiravir was confirmed with a mean lung to plasma ratio ranging from 0.35 to 0.44. Favipiravir was
200 not detected in the lungs at the lowest dose (18.75mg/day).

201 **Table 3: Plasma and lung concentrations of favipiravir after administration of a single dose or multiple**
202 **dose of favipiravir**

	Single Dose			Multiple Dose ¹ (Day 3)		
	Plasma (μ g/mL)	Lung (μ g/g)	L/p ratio	Plasma (μ g/mL)	Lung (μ g/g)	L/p ratio
Dose: 25 mg					Dose : 75mg/day TID	
0.5 hr	372 \pm 47.5	216 \pm 39	0.58 \pm 0,04			
1 hr	279 \pm 49.9					
5 hr	135 \pm 49.0	81,3 \pm 24	0.62 \pm 0,10			
8 hr	5.77 \pm 1.34					
12 hr	1.43 ²			29.9 \pm 9.83	16.0 \pm 4.87	0.44 \pm 0,07
Dose: 12.5 mg					Dose : 37.5mg/day TID	
0.5 hr	166 \pm 52.0	90.7 \pm 12.7	0.58 \pm 0.14			
1 hr	155 \pm 20.6					
5 hr	10.7 \pm 5.16	3.84 \pm 1.49	0.37 \pm 0.052			
8 hr	1.94 \pm 0.06					
12 hr	0.16 ²			2.57 \pm 1.22	1.36 \pm 0.14	0.35 \pm 0,03
Dose: 6.25 mg					Dose :18.75mg/day TID	
0.5 hr	86.3 \pm 4.11	50.2 \pm 16.4	0.58 \pm 0.17			
1 hr	35.2 \pm 27.8					
5 hr	2.90 \pm 0.25	1.09 \pm 0.05	0.38 \pm 0.05			
8 hr	0.56 \pm 0.16					
12 hr	0.05 ²			0.31 \pm 0.14	not detected	<i>n.a.</i>

203 Data represent mean \pm SD; Three animals for each condition except at multiple dose (n=9 for plasma; n=3 for
204 lung); details in Table S5

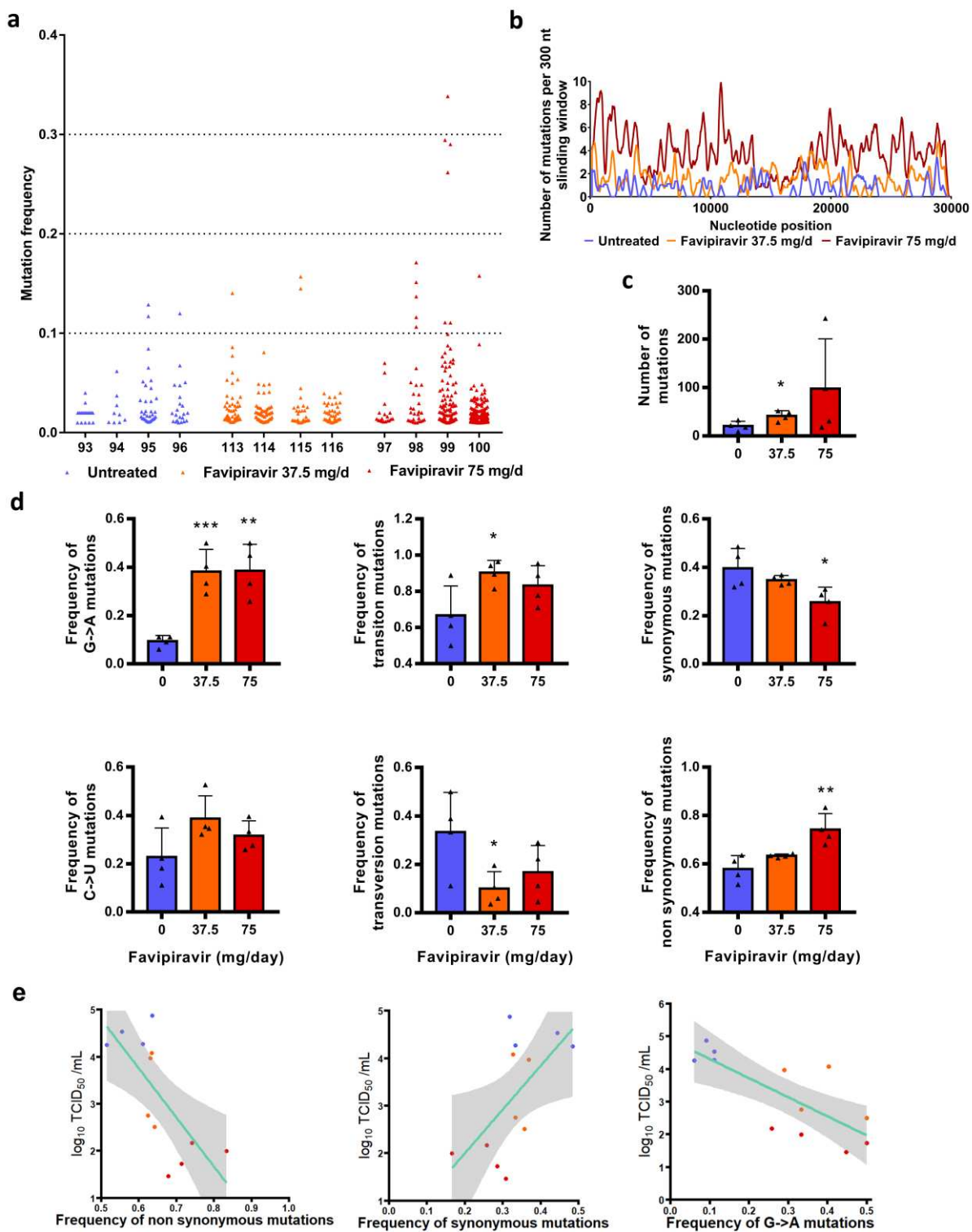
205 ¹: PK realized after 3 days of favipiravir administered three times a day

206 ²: extrapolated C_{12h}. *na*: not applicable

207 **Mutagenic effect of favipiravir**

208 To understand which genomic modifications accompanied favipiravir treatment, direct complete
209 genome sequencing of clarified lung homogenates from animals intranasally infected with 10^6 TCID₅₀
210 of virus and treated with the two highest doses of drug (preemptive antiviral therapy; Figure 2) was
211 performed. Data were generated by next generation sequencing from lung samples of four animals
212 per group (untreated, 37.5mg/day TID and 75mg/day TID). The mean sequencing coverage for each
213 sample ranged from 10,991 to 37,991 reads per genomic position and we subjected substitutions with
214 a frequency $\geq 1\%$ to further analysis. The genetic variability in virus stock was also analyzed: 14
215 nucleotide polymorphisms were detected of which 5 recorded a mutation frequency higher than 10%
216 (Table S6).

217 In order to study the mutagenic effect of favipiravir, we used the consensus sequence from virus stock
218 as reference and all the mutations simultaneously detected in a lung sample and in virus stock were
219 not considered in the further analysis (1 to 4 mutations per sample, see Table S6). Overall, no majority
220 mutations were detected (mutation frequency $> 50\%$), mutations were distributed throughout the
221 whole genome and almost all of them exhibited a frequency lower than 10% (Figure 5a and 5b).
222 Results revealed a relationship between the number of mutations detected per sample and the dose
223 of favipiravir (Figure 5c): the mean number of mutations increased by a factor 2 and 4.8 with groups
224 of animals treated with 37.5 and 75mg/day TID, respectively. The difference is significant only with a
225 dose of 37.5mg/day TID ($p=0.029$). This increase of the number of mutations is mainly the consequence
226 of the occurrence of a large number of G→A substitutions and, to a lesser extent, C→U substitutions.
227 Consequently, regardless of the dose of favipiravir, mean frequency of G→A substitutions was
228 significantly increased by a factor of 4.2 ($p\leq 0.009$). This rise of these transition mutations led to
229 increased frequency of all transition mutations (significant only at dose of 37.5mg/day TID; $p=0.037$)
230 and increased frequency of non-synonymous mutations (significant only at dose of 75mg/day TID;
231 $p=0.009$) (Figure 5d). We investigated whether or not effectiveness in treated animals was linked with
232 the characteristics of the mutations detected on viral populations and found that infectious titers in
233 lungs were negatively associated with frequency of non-synonymous and G→A mutations, and
234 positively associated with frequency of synonymous mutations ($p<0.03$; Figure 5e). Finally, our
235 experiments revealed some parallel evolution events; 32 substitutions in viral sub-populations were
236 detected in two independent animals. Notably, 18 of these shared mutations were detected only with
237 treated animals, 14 of them being non-synonymous (Table S8). These mutations are located in nsp2,
238 3, 4, 5, 6, 14, N protein, Matrix, ORF 3a and 8. At this stage, one cannot conclude if these substitutions
239 reflect the adaptation to the hamster model or are the result of the antiviral selection.



240

241 **Figure 5: Mutagenic effect of favipiravir**

242 a Viral genetic diversity in clarified lung homogenates. For each condition, four samples were analyzed. Each
 243 triangle represents a mutation (only substitutions with a frequency $\geq 1\%$ were considered). b Patterns of mutation
 244 distribution on complete viral genome. Each variable nucleotide position was counted only once when found.
 245 The variability was represented using 75 nt sliding windows. For each condition, variable nucleotide positions
 246 were determined and represented using a 300 nt sliding window. c Mean number of mutations. Data represent

247 mean \pm SD. **d** Mutation characteristics. For each sample, the frequency of a given mutation was calculated as
248 follows: number of this kind of mutation detected in the sample divided by the total number of mutations
249 detected in this sample. Data represent mean \pm SD. ** and * symbols indicate that the average value for the group
250 is significantly different from that of the untreated group with a p-value ranging between 0.001-0.01 and 0.01-
251 0.05 respectively (details in details in Table S6 and S7). **e** Association between lung infectious titers (measured
252 using a TCID₅₀ assay) and frequency of non synonymous, synonymous and G \rightarrow A mutations. Each dot represent
253 data from a given animal.

254 **Discussion**

255 In the current study, we used a hamster model to assess efficacy of the favipiravir against SARS-CoV-
256 2. Following infection, viral RNA was mainly detected in lungs, blood, and, to a lesser extent, in the
257 large bowel. Peak of viral replication was observed at 2-3 dpi followed by observation of significant
258 weight losses, in line with recently reported investigations that involved 6-10 weeks old hamsters^{7,21}.
259 Clinically, the main symptom was weight loss, observed from the first day of infection and followed by
260 recovery at 6dpi. This confirmed that the *in vivo* model, with younger animals (4 weeks-old), is suitable
261 for preclinical evaluation of antiviral compounds against SARS-CoV-2.

262 Using a preemptive strategy, we demonstrated that doses of favipiravir of around 700-1400mg/kg/day
263 TID reduced viral replication in lungs of infected animals and allowed clinical alleviation of the disease.
264 In the most favourable situation, where high doses were used as a preventive therapy, favipiravir led
265 to undetectable viral replication in lung and plasma. These results showed that the use of high doses
266 of favipiravir could expand its *in vivo* spectrum against RNA viruses.

267 Reduction of viral replication was greater when estimated on the basis of infectious titers than on total
268 viral RNA as previously observed in non-human primates treated with Remdesivir²². However, the
269 effective doses of favipiravir were higher than those usually used in rodent models (\approx 100-
270 400mg/kg/day)^{10,12,23-26}. This can be correlated with the high favipiravir EC₅₀ found *in vitro* for SARS-
271 CoV-2. Moreover, effective doses were associated with significant toxicity in our hamster model. This
272 observed toxicity reflected only the adverse effects of favipiravir and was not exacerbated during SARS-
273 CoV-2 infection. Indeed, similar weight losses were measured among infected and non-infected
274 animals treated with the highest dose of favipiravir at 1, 2 and 3dpi.

275 In the present study, reduction of viral replication was correlated with the dose of favipiravir
276 administrated and inversely correlated with the dose of virus inoculated. In a recent study, favipiravir
277 administrated *per os* twice daily (loading dose of 600mg/kg/day followed by 300mg/kg/day) revealed
278 a mild reduction of lung viral RNA yields using a similar hamster model with high doses of virus (2×10^6
279 TCID₅₀)²¹. These results are in accordance with ours at the lower dose of favipiravir (around
280 340mg/kg/day TID).

281 With influenza viruses, favipiravir acts as a nucleotide analogue. It is metabolized intracellularly to its
282 active form and incorporated into nascent viral RNA strands. This inhibits RNA strand extension and
283 induces abnormal levels of mutation accumulation into the viral genome^{16,17}. Recently, it was shown
284 *in vitro* that favipiravir has a similar mechanism of action with SARS-CoV-2 through a combination of
285 chain termination, reduced RNA synthesis and lethal mutagenesis²⁰. Our genomic analysis confirmed
286 the mutagenic effect of favipiravir *in vivo*. Indeed, we found that favipiravir treatment induced

287 appearance of a large number of G → A and C → U mutations into viral genomes. This was associated to
288 a decrease of viral infectivity probably because alteration of the genomic RNA disturb the replication
289 capacity. Similar findings were described *in vitro* and *in vivo* with other RNA viruses^{9,16,27,28}. Of note, we
290 also observed a strong inverse association between infectious titers in lungs and the proportion of
291 non-synonymous mutations detected in viral populations. Because random non-synonymous
292 mutations are more deleterious than synonymous mutations²⁹, this suggests that they were randomly
293 distributed over the three positions of the codons and that no compensatory mechanism was triggered
294 by the virus to eliminate them (*i.e.* negative selection). Finally, the inverse correlation between lung
295 infections titers and the frequency of G → A substitutions showed that an increased proportion of these
296 mutations beyond an error threshold might be expected to cause lethal mutagenesis.

297 Genomic analyses revealed that 18 mutations detected in viral sub-populations were shared only with
298 treated animals. Two of them were located in the nsp14 coding region involved in the proof-reading
299 activity of the viral RNA polymerisation^{30,31}. However, they were located in the N7 MTase domain
300 involved in viral RNA capping^{32,33}. By comparison, resistance mutations selected against Remdesivir in
301 β-coronavirus murine hepatitis virus model were obtained in the RdRP (nsp12) coding sequence³⁴.
302 Further investigations are needed to assess the impact of these mutations on the antiviral effect of
303 favipiravir.

304 Favipiravir PK in our hamster model displayed a non-linear increase in plasma exposure between the
305 doses as already reported in nonhuman primates³⁵. The observed favipiravir concentration versus time
306 profiles were in agreement with previous results of a PK study performed in 7-8 week-old hamsters
307 orally treated with a single dose of 100mg/kg of favipiravir³⁶. The maximum plasma drug concentration
308 occurred at 0.5 h after oral administration, earlier than in humans, and then decreased rapidly in
309 agreement with its short half-life³⁷. After repeated doses, plasma exposure confirmed non-linear PK
310 over the entire range of doses, further emphasized by accumulation ratios. The important
311 accumulation observed at the highest dose could explain in part the toxicity observed in hamsters at
312 this dose. Favipiravir undergoes an important hepatic metabolism mainly by aldehyde oxidase
313 producing an inactive M1 metabolite and inhibits aldehyde oxidase activity in a concentration- and
314 time-dependent manner. These properties explain the self-inhibition of its own metabolism as
315 observed in our study in which the highest dose of favipiravir led to a greater increase in favipiravir
316 concentrations³⁸.

317 A good penetration of favipiravir in lungs was observed with lung/plasma ratios ranging from 35 to
318 44% after repeated doses, consistent with its physicochemical properties. Lung exposure was also in
319 accordance with previous studies³⁶.

320 The medium dose of favipiravir used in this study (670mg/kg/day TID) is within the range of the
321 estimated doses required to reduce by 90% (ED90) the level of infectious titers in lungs (ranging
322 between 570 and 780mg/kg/day). Animals treated with this dose displayed significant reduction of
323 viral replication in lungs, limited drug-associated toxicity and clinical alleviation of the disease.
324 Regarding the accumulation ratio after repeated doses and the good penetration of favipiravir in lungs,
325 effective concentrations can be expected in lungs, throughout the course of treatment using this dose
326 of 670mg/kg/day TID.

327 How clinically realistic are these results? To address this question we compared the drug
328 concentrations obtained in the hamster model with those obtained in patients. In 2016, a clinical trial
329 evaluated the use of favipiravir in Ebola infected patients³⁹. The dose used in Ebola infected patients
330 was 6000mg on day 0 followed by 1200mg BID for 9 days. The median trough concentrations of
331 favipiravir at Day 2 and Day 4 were 46.1 and 25.9 μ g/mL, respectively. This is within the range observed
332 here in hamsters treated with the highest dose (around 1400mg/kg/day), with a mean trough
333 concentration of 29.9 μ g/mL. However, additional investigations are required to determine whether or
334 not similar favipiravir plasma exposure in SARS-CoV-2 infected patients are associated with antiviral
335 activity. The major differences in PK between hamster and humans, and the toxicity observed at the
336 highest doses in our animal model limits the extrapolation of our results. Therefore, whether safe
337 dosing regimens in humans may achieve similar plasma exposure and recapitulate the profound effect
338 on viral replication is unknown. Further, the intracellular concentration of the active metabolite was
339 not determined and which parameter of the drug pharmacokinetics best drives the antiviral effect
340 remains to be established.

341 In summary, this study establishes that high doses of favipiravir are associated with antiviral activity
342 against SARS-CoV-2 infection in a hamster model. The better antiviral efficacy was observed using a
343 preventive strategy, suggesting that favipiravir could be more appropriate for a prophylactic use. Our
344 results should be interpreted with caution because high doses of favipiravir were associated with signs
345 of toxicity in our model. It is required to determine if a tolerable dosing regimen could generate similar
346 exposure in non-human primates, associated with significant antiviral activity, before testing a high
347 dose regimen in COVID-19 patients. Furthermore, subsequent studies should determine if an increased
348 antiviral efficacy can be reached using favipiravir in association with other effective antiviral drugs,
349 since this strategy may enable to reduce the dosing regimen of favipiravir. Finally, this work reinforces
350 the need for rapid development of animal models to confirm *in vivo* efficacy of antiviral compounds
351 and accordingly, to determine appropriate dose regimens in humans before starting clinical trials.

352 **Methods**

353 **Cells**

354 VeroE6 cells (ATCC CRL-1586) and Caco-2 cells (ATCC HTB-37) were grown at 37°C with 5% CO₂ in
355 minimal essential medium (MEM) supplemented with 7.5% heat-inactivated fetal bovine serum (FBS),
356 1% Penicillin/Streptomycin and 1% non-essential amino acids (all from ThermoFisher Scientific).

357 **Virus**

358 All experiments with infectious virus were conducted in biosafety level (BSL) 3 laboratory. SARS-CoV-2
359 strain BavPat1, supplied through European Virus Archive GLOBAL (<https://www.european-virus-archive.com/>), was provided by Christian Drosten (Berlin, Germany). Virus stocks were prepared by
360 inoculating at MOI of 0.001 a 25cm² culture flask of confluent VeroE6 cells with MEM medium
361 supplemented with 2.5% FBS. The cell supernatant medium was replaced each 24h hours and
362 harvested at the peak of infection, supplemented with 25mM HEPES (Sigma), aliquoted and stored at
363 -80°C.

365 ***In vitro* determination of EC₅₀, EC₉₀, CC₅₀ and infectious titer reductions**

366 One day prior to infection, 5×10⁴ VeroE6 cells were seeded in 96-well culture plates (5×10⁴ cells/well
367 in 100µL of 2.5% FBS medium (assay medium). The next day, seven 2-fold serial dilutions of favipiravir
368 (Courtesy of Toyama-Chemical; 0.61µg/mL to 78.5µg/mL, in triplicate) were added (25µL/well, in assay
369 medium). Eight virus control wells were supplemented with 25µL of assay medium and eight cell
370 controls were supplemented with 50µL of assay medium. After 15 min, 25µL of virus suspension,
371 diluted in assay medium, was added to the wells at an MOI of 0.01 or 0.001 (except for cell controls).
372 Three days after infection, cell supernatant media were collected to perform TCID₅₀ assay (at
373 concentration of 78.5, 39.3, 19.6µg/mL), as described below, in order to calculate infectious titer
374 reductions and cell viability was assessed using CellTiter-Blue reagent (Promega) following
375 manufacturer's instructions. Fluorescence (560/590nm) was recorded with a Tecan Infinite 200Pro
376 machine (Tecan). The 50% and 90% effective concentrations (EC₅₀, EC₉₀) were determined using
377 logarithmic interpolation (% of inhibition were calculated as follows: (OD_{sample}-OD_{virus control})/(OD_{cell control}-
378 OD_{virus control})). For the evaluation of CC₅₀ (the concentration that induced 50% cytotoxicity), the same
379 culture conditions were set as for the determination of the EC₅₀, without addition of the virus, then
380 cell viability was measured using CellTiter Blue (Promega). CC₅₀ was determined using logarithmic
381 interpolation.

382 *In vivo experiments*

383 Approval and authorization

384 *In vivo experiments* were approved by the local ethical committee (C2EA—14) and the French
385 ‘Ministère de l’Enseignement Supérieur, de la Recherche et de l’Innovation’ (APAFIS#23975) and
386 performed in accordance with the French national guidelines and the European legislation covering
387 the use of animals for scientific purposes. All experiments were conducted in BSL 3 laboratory.

388 Animal handling

389 Three-week-old female Syrian hamsters were provided by Janvier Labs. Animals were maintained in
390 ISOcage P - Bioexclusion System (Techniplast) with unlimited access to water/food and 14h/10h
391 light/dark cycle. Animals were weighed and monitored daily for the duration of the study to detect the
392 appearance of any clinical signs of illness/suffering. Virus inoculation was performed under general
393 anesthesia (isoflurane). Organs and blood were collected after euthanasia (cervical dislocation) which
394 was also realized under general anesthesia (isofluorane).

395 Hamster Infection

396 Anesthetized animals (four-week-old) were intranasally infected with 50µL containing 10^6 , 10^5 or
397 10^4 TCID₅₀ of virus in 0.9% sodium chloride solution). The mock group was intranasally inoculated with
398 50µL of 0.9% sodium chloride solution.

399 Favipiravir administration

400 Hamster were intra-peritoneally inoculated with different doses of favipiravir. Control group were
401 intra-peritoneally inoculated with a 0.9% sodium chloride solution.

402 Organ collection

403 Organs were first washed in 10mL of 0.9% sodium chloride solution and then transferred to a 2mL or
404 50mL tube containing respectively 1mL (small/large bowel pieces, kidney, spleen and heart) or 10mL
405 (lungs, brain and liver) of 0.9% sodium chloride solution and 3mm glass beads. They were crushed
406 using a the Tissue Lyser machine (Retsch MM400) for 5min at 30 cycles/s and then centrifuged 5min à
407 1200g. Supernatant media were transferred to a 2mL tube, centrifuged 10 min at 16,200g and stored
408 at -80°C. One milliliter of blood was harvested in a 2mL tube containing 100µL of 0.5M EDTA
409 (ThermoFischer Scientific). Blood was centrifuged for 10 min at 16,200g and stored at -80°C.

410 Quantitative real-time RT-PCR (RT-qPCR) assays

411 To avoid contamination, all experiments were conducted in a molecular biology laboratory that is
412 specifically designed for clinical diagnosis using molecular techniques, and which includes separate
413 laboratories dedicated to perform each step of the procedure. Prior to PCR amplification, RNA
414 extraction was performed using the QIAamp 96 DNA kit and the Qiacube HT kit and the Qiacube HT

415 (both from Qiagen) following the manufacturer's instructions. Shortly, 100 μ L of organ clarified
416 homogenates, spiked with 10 μ L of internal control (bacteriophage MS2)⁴⁰, were transferred into an S-
417 block containing the recommended volumes of VXL, proteinase K and RNA carrier. RT-qPCR (SARS-CoV-
418 2 and MS2 viral genome detection) were performed with the Express one step RT-qPCR Universal kit
419 (ThermoFisher Scientific) using 3.5 μ L of RNA and 6.5 μ L of RT-qPCR mix that contains 250nmol of each
420 primer and 75nmol of probe. Amplification was performed with the QuantStudio 12K Flex Real-Time
421 PCR System (ThermoFisher Scientific) using the following conditions: 50°C for 10min, 95°C for 20s,
422 followed by 40 cycles of 95°C for 3s, 60°C for 30s. qPCR (γ -actine gene detection) was perfomed under
423 the same condition as RT-qPCR with the following modifications: we used the Express one step qPCR
424 Universal kit (ThermoFisher Scientific) and the 50°C step of the amplification cycle was removed.
425 Primers and probes sequences used to detect SARS-CoV-2, MS2 and γ -actine are described in Table S9.

426 **Tissue-culture infectious dose 50 (TCID₅₀) assay**

427 To determine infectious titers, 96-well culture plates containing confluent VeroE6 cells were
428 inoculated with 150 μ L per well of serial dilutions of each sample (four-fold or ten-fold dilutions when
429 analyzing lung clarified homogenates or cell supernatant media respectively). Each dilution was
430 performed in sextuplicate. Plates were incubated for 4 days and then read for the absence or presence
431 of cytopathic effect in each well. Infectious titers were estimated using the method described by Reed
432 & Muench⁴¹.

433 **Favipiravir pharmacokinetics**

434 Animal handling, hamster infections and favipiravir administrations were performed as described
435 above. A piece of left lung was first washed in 10mL of sodium chloride 0.9% solution, blotted with
436 filter paper, weighed and then transferred to a 2mL tube containing 1mL of 0.9% sodium chloride
437 solution and 3mm glass beads. It was crushed using the Tissue Lyser machine (Retsch MM400) during
438 10min at 30 cycles/s and then centrifuged 5min à 1200g. Supernatant media were transferred to 2mL
439 tubes, centrifuged 10 min at 16,200g and stored at -80°C. One milliliter of blood was harvested in a
440 2mL tube containing 100 μ L of 0.5M EDTA (ThermoFischer Scientific). Blood was centrifuged for 10 min
441 at 16,200g and stored at -80°C.

442 Quantification of favipiravir in plasma and lung tissues was performed by a validated sensitive and
443 selective validated high-performance liquid chromatography coupled with tandem mass spectrometry
444 method (UPLC-TQD, Waters, USA) with a lower limit of quantification of 0.1 μ g/mL. Precision and
445 accuracy of the 3 quality control samples (QCs) were within 15% over the calibration range (0.5 μ g/mL
446 to 100 μ g/mL) (Bekegnran *et al.*, submitted). Favipiravir was extracted by a simple protein precipitation
447 method, using acetonitrile for plasma and ice-cold acetonitrile for clarified lung homogenates. Briefly,
448 50 μ L of samples matrix was added to 500 μ L of acetonitrile solution containing the internal standard

449 (favipiravir-13C,15N, Alsachim), then vortexed for 2min followed by centrifugation for 10min at 4°C.
450 The supernatant medium was evaporated and the dry residues were then transferred to 96-well plates
451 and 50 µL was injected. To assess the selectivity and specificity of the method and matrix effect, blank
452 plasma and tissues homogenates from 2 control animals (uninfected and untreated) were processed
453 at each run. Moreover, the same control samples spiked with favipiravir concentration equivalent to
454 the QCs (0.75, 50 and 80 µg/mL) were also processed and compared to the QCs samples.
455 Noncompartmental analysis conducted using software Pkanalix2019R2 (www.lixoft.com). Areas
456 under the plasma concentration time curve were computed using medians of favipiravir
457 concentrations at 0.5, 1, 5 and 8 hours, and extrapolated until T=12h. C_{trough} were extrapolated at
458 T=12h using lambda-z loglinear regression on the decreasing slope of concentrations.

459 Sequence analysis of the full-length genome

460 200µL of lung clarified homogenate or infectious cell supernatant (virus stock) was inactivated with an
461 equal volume of VXL lysis buffer (Qiagen) and viral RNA was extracted using an EZ1 Advanced XL robot
462 with the EZ1 mini virus 2.0 kit (both from Qiagen) and linear acrylamide (ThermoFisher Scientific) in
463 place of carrier RNA. cDNA was generated in a final volume of 40µL using 14µL of nucleic acid extract,
464 random hexamer and the Protoscript II First Strand cDNA Synthesis Kit (New England Biolabs). A
465 specific set of primers (Table S10) was used to generate thirteen amplicons covering the entire genome
466 with the Q5 High-Fidelity DNA polymerase (New England Biolabs). PCR mixes (final volume 25µL)
467 contained 2.5µL of cDNA, 2µL of each primer (10µM) and 12.5 µL of Q5 High-Fidelity 2X Master Mix.
468 Amplification was performed with the following conditions: 30 sec at 98°C, then 45 cycles of 15 sec at
469 98°C and 5 min à 65°C. Size of PCR products was verified by gel electrophoresis. For each sample, an
470 equimolar pool of all amplicons was prepared and purified using Monarch PCR & DNA Cleanup Kit (New
471 England Biolabs). After DNA quantification using Qubit dsDNA HS Assay Kit and Qubit 2.0 fluorometer
472 (ThermoFisher Scientific), amplicons were fragmented by sonication into fragments of around 200bp
473 long. Libraries were built by adding barcodes, for sample identification, and primers using AB Library
474 Builder System (ThermoFisher Scientific). To pool equimolarly the barcoded samples a quantification
475 step by real time PCR using Ion Library TaqMan Quantitation Kit (ThermoFisher Scientific) was
476 performed. Then, emulsion PCR from pools and loading on 530 chip was performed using the
477 automated Ion Chef instrument (ThermoFisher Scientific). Sequencing was performed using the S5 Ion
478 torrent technology v5.12 (ThermoFisher Scientific) following manufacturer's instructions. Consensus
479 sequence was obtained after trimming of reads (reads with quality score <0.99, and length <100pb
480 were removed and the 30 first and 30 last nucleotides were removed from the reads). Mapping of the
481 reads on a reference (determine following blast of De Novo contigs) was done using CLC genomics
482 workbench software v.20 (Qiagen). A *de novo* contig was also produced to ensure that the consensus

483 sequence was not affected by the reference sequence. Mutation frequency for each position was
484 calculated as the number of reads with a mutation compared to the reference divided by the total
485 number of reads at that site. Only substitutions with a frequency of at least 1% were taken into account
486 for the analysis (Table S6).

487 **ED₅₀, ED₉₀ and ED₉₉ determination**

488 We conducted a nonlinear regression of infectious viral load against dose, using an E_{max} model, giving

489
$$= \frac{o \times (1 - (1 + \frac{d}{D_50}))}{D_50}$$
 with o being infectious viral load of untreated animals. We estimated
490 D_50 the dose required to decrease viral load by 50%, using a coefficient to account for the high
491 sigmoidicity of the relation between dose and titers. coefficient was chosen as the one maximizing
492 likelihood of the model. We extrapolated the D_{50} and D_{99} using $D_{50} = \frac{9 \times D_{50}}{99}$ and $D_{99} =$
493 $\frac{99 \times D_{50}}{99}$ as well as their 95% confidence interval using the delta method.

494 **Statistical analysis**

495 Graphical representations and statistical analyses were performed with Graphpad Prism 7 (Graphpad
496 software) except linear/nonlinear regressions and their corresponding graphical representations that
497 were performed using R statistical software (<http://www.R-project.org>). Statistical details for each
498 experiments are described in the figure legends and in corresponding supplemental tables. P-values
499 lower than 0.05 were considered statistically significant.

500

501 **Acknowledgments**

502 We thank Laurence Thirion (UVE; Marseille) for providing RT-qPCR systems . We thank Camille Placidi
503 (UVE; Marseille) for her technical contribution. We also thank Pr. Ernest A. Gould (UVE; Marseille) for
504 his careful reading of the manuscript and English language editing. We thank Pr Drosten and Pr Drexler
505 for providing the SARS-CoV-2 strain through the European Research infrastructure EVA GLOBAL. This
506 work was supported by the Fondation de France “call FLASH COVID-19”, project TAMAC, by “Institut
507 national de la santé et de la recherche médicale” through the REACTing (REsearch and ACTion targeting
508 emerging infectious diseases) initiative (“Preuve de concept pour la production rapide de virus
509 recombinant SARS-CoV-2”), and by European Virus Archive Global (EVA 213 GLOBAL) funded by the
510 European Union’s Horizon 2020 research and innovation program under grant agreement No. 871029.
511 A part of the work was done on the Aix Marseille University antivirals platform “AD2P”.

512 **Author Contributions**

513 Conceptualization, J.S.D., M.C., G.M. and A.N. ; Methodology, J.S.D., M.C., G.L., G.M. and A.N. ; Formal
514 Analysis, J.S.D., M.C. and G.L. ; Investigation, J.S.D., M.C., G.M., F.T., P.R.P., G.P., K.B. and A.N. ;
515 Resources, F.T., B.C., J.G., X.d.L., C.S. and A.N. ; Writing – Original Draft, J.S.D., M.C., J.G., C.S. and A.N.
516 ; Writing – Review & Editing, J.G., X.d.L., C.S. and A.N. ; Visualization, J.S.D., M.C., G.L., F.T., P.R.P. and
517 A.N. ; Supervision, A.N. ; Funding Acquisition, F.T., B.C., X.d.L. and A.N.

518 **Competing Interests**

519 J.G has consulted for F. Hoffman-La Roche. C.S has consulted for ViiV Healthcare, MSD and Gilead. The
520 remaining authors declare no competing interests.

521 **Materials & Correspondence**

522 Correspondence to Antoine Nougairède.

523 **Supplemental Data**

524 Supplemental figure 1: In vitro efficacy of favipiravir

525 Supplemental figure 2: Dose-response curves

526 Supplemental figure 3: Evaluation of the toxicity for animals infected and treated with high doses of

527 favipiravir

528 Supplemental figure 4: Plasma concentrations of favipiravir after administration of a single dose of

529 favipiravir

530 Supplemental table 1: Implementation of hamster model

531 Supplemental table 2: Individual data from in vivo experiments

532 Supplemental table 3: Statistical analysis of in vivo experiments

533 Supplemental table 4: Statistical analysis of clinical monitoring

534 Supplemental table 5: Individual data of favipiravir pharmacokinetics

535 Supplemental table 6: Individual data for analysis of mutagenic effect of favipiravir

536 Supplemental table 7: Statistical analysis of mutagenic effect of favipiravir

537 Supplemental table 8: Shared mutations detected in lung clarified homogenates

538 Supplemental table 9: (RT)-qPCR systems

539 Supplemental table 10: Primer sequences used to produce overlapping amplicons for next generation

540 sequencing

541 **References**

542 1 WHO. World Health Organization. WHO Director-General's opening remarks at the media
543 briefing on COVID-19 - 11 March 2020 (<https://www.who.int>). (2020).

544 2 Zhu, N. *et al.* A Novel Coronavirus from Patients with Pneumonia in China, 2019. *N Engl J Med*
545 **382**, 727-733, doi:10.1056/NEJMoa2001017 (2020).

546 3 Huang, C. *et al.* Clinical features of patients infected with 2019 novel coronavirus in Wuhan,
547 China. *Lancet* **395**, 497-506, doi:10.1016/S0140-6736(20)30183-5 (2020).

548 4 He, X. *et al.* Temporal dynamics in viral shedding and transmissibility of COVID-19. *Nat Med*
549 **26**, 672-675, doi:10.1038/s41591-020-0869-5 (2020).

550 5 Dong, E., Du, H. & Gardner, L. An interactive web-based dashboard to track COVID-19 in real
551 time. *Lancet Infect Dis* **20**, 533-534, doi:10.1016/S1473-3099(20)30120-1 (2020).

552 6 Mercorelli, B., Palu, G. & Lorean, A. Drug Repurposing for Viral Infectious Diseases: How Far
553 Are We? *Trends Microbiol* **26**, 865-876, doi:10.1016/j.tim.2018.04.004 (2018).

554 7 Chan, J. F. *et al.* Simulation of the clinical and pathological manifestations of Coronavirus
555 Disease 2019 (COVID-19) in golden Syrian hamster model: implications for disease
556 pathogenesis and transmissibility. *Clin Infect Dis*, doi:10.1093/cid/ciaa325 (2020).

557 8 Rockx, B. *et al.* Comparative pathogenesis of COVID-19, MERS, and SARS in a nonhuman
558 primate model. *Science* **368**, 1012-1015, doi:10.1126/science.abb7314 (2020).

559 9 Guedj, J. *et al.* Antiviral efficacy of favipiravir against Ebola virus: A translational study in
560 cynomolgus macaques. *PLoS Med* **15**, e1002535, doi:10.1371/journal.pmed.1002535 (2018).

561 10 Yamada, K. *et al.* Reevaluation of the efficacy of favipiravir against rabies virus using in vivo
562 imaging analysis. *Antiviral Res* **172**, 104641, doi:10.1016/j.antiviral.2019.104641 (2019).

563 11 Segura Guerrero, N. A., Sharma, S., Neyts, J. & Kaptein, S. J. F. Favipiravir inhibits in vitro Usutu
564 virus replication and delays disease progression in an infection model in mice. *Antiviral Res*
565 **160**, 137-142, doi:10.1016/j.antiviral.2018.10.026 (2018).

566 12 Tani, H. *et al.* Therapeutic effects of favipiravir against severe fever with thrombocytopenia
567 syndrome virus infection in a lethal mouse model: Dose-efficacy studies upon oral
568 administration. *PLoS One* **13**, e0206416, doi:10.1371/journal.pone.0206416 (2018).

569 13 Jochmans, D. *et al.* Antiviral Activity of Favipiravir (T-705) against a Broad Range of
570 Paramyxoviruses In Vitro and against Human Metapneumovirus in Hamsters. *Antimicrob
571 Agents Chemother* **60**, 4620-4629, doi:10.1128/AAC.00709-16 (2016).

572 14 Takahashi, K. *et al.* In vitro and in vivo activities of T-705 and oseltamivir against influenza virus.
573 *Antivir Chem Chemother* **14**, 235-241, doi:10.1177/095632020301400502 (2003).

574 15 Rosenke, K. *et al.* Use of Favipiravir to Treat Lassa Virus Infection in Macaques. *Emerg Infect
575 Dis* **24**, 1696-1699, doi:10.3201/eid2409.180233 (2018).

576 16 Baranovich, T. *et al.* T-705 (favipiravir) induces lethal mutagenesis in influenza A H1N1 viruses
577 in vitro. *J Virol* **87**, 3741-3751, doi:10.1128/JVI.02346-12 (2013).

578 17 Sangawa, H. *et al.* Mechanism of action of T-705 ribosyl triphosphate against influenza virus
579 RNA polymerase. *Antimicrob Agents Chemother* **57**, 5202-5208, doi:10.1128/AAC.00649-13
580 (2013).

581 18 Wang, M. *et al.* Remdesivir and chloroquine effectively inhibit the recently emerged novel
582 coronavirus (2019-nCoV) in vitro. *Cell Res* **30**, 269-271, doi:10.1038/s41422-020-0282-0
583 (2020).

584 19 Jeon, S. *et al.* Identification of antiviral drug candidates against SARS-CoV-2 from FDA-
585 approved drugs. *Antimicrob Agents Chemother*, doi:10.1128/AAC.00819-20 (2020).

586 20 Shannon, A. *et al.* Favipiravir strikes the SARS-CoV-2 at its Achilles heel, the RNA polymerase.
587 *bioRxiv*, 2020.2005.2015.098731, doi:10.1101/2020.05.15.098731 (2020).

588 21 Kaptein, S. J. *et al.* Antiviral treatment of SARS-CoV-2-infected hamsters reveals a weak effect
589 of favipiravir and a complete lack of effect for hydroxychloroquine. *bioRxiv*,
590 2020.2006.2019.159053, doi:10.1101/2020.06.19.159053 (2020).

591 22 Williamson, B. N. *et al.* Clinical benefit of remdesivir in rhesus macaques infected with SARS-
592 CoV-2. *Nature*, doi:10.1038/s41586-020-2423-5 (2020).

593 23 Sidwell, R. W. *et al.* Efficacy of orally administered T-705 on lethal avian influenza A (H5N1)
594 virus infections in mice. *Antimicrob Agents Chemother* **51**, 845-851, doi:10.1128/AAC.01051-
595 06 (2007).

596 24 Smither, S. J. *et al.* Post-exposure efficacy of oral T-705 (Favipiravir) against inhalational Ebola
597 virus infection in a mouse model. *Antiviral Res* **104**, 153-155,
598 doi:10.1016/j.antiviral.2014.01.012 (2014).

599 25 Julander, J. G., Shafer, K., Smee, D. F., Morrey, J. D. & Furuta, Y. Activity of T-705 in a hamster
600 model of yellow fever virus infection in comparison with that of a chemically related
601 compound, T-1106. *Antimicrob Agents Chemother* **53**, 202-209, doi:10.1128/AAC.01074-08
602 (2009).

603 26 Oestereich, L. *et al.* Efficacy of Favipiravir Alone and in Combination With Ribavirin in a Lethal,
604 Immunocompetent Mouse Model of Lassa Fever. *J Infect Dis* **213**, 934-938,
605 doi:10.1093/infdis/jiv522 (2016).

606 27 Escribano-Romero, E., Jimenez de Oya, N., Domingo, E. & Saiz, J. C. Extinction of West Nile
607 Virus by Favipiravir through Lethal Mutagenesis. *Antimicrob Agents Chemother* **61**,
608 doi:10.1128/AAC.01400-17 (2017).

609 28 Arias, A., Thorne, L. & Goodfellow, I. Favipiravir elicits antiviral mutagenesis during virus
610 replication in vivo. *Elife* **3**, e03679, doi:10.7554/elife.03679 (2014).

611 29 Cuevas, J. M., Domingo-Calap, P. & Sanjuan, R. The fitness effects of synonymous mutations in
612 DNA and RNA viruses. *Mol Biol Evol* **29**, 17-20, doi:10.1093/molbev/msr179 (2012).

613 30 Eckerle, L. D., Lu, X., Sperry, S. M., Choi, L. & Denison, M. R. High fidelity of murine hepatitis
614 virus replication is decreased in nsp14 exoribonuclease mutants. *J Virol* **81**, 12135-12144,
615 doi:10.1128/JVI.01296-07 (2007).

616 31 Ferron, F. *et al.* Structural and molecular basis of mismatch correction and ribavirin excision
617 from coronavirus RNA. *Proc Natl Acad Sci U S A* **115**, E162-E171, doi:10.1073/pnas.1718806115
618 (2018).

619 32 Chen, Y. *et al.* Structure-function analysis of severe acute respiratory syndrome coronavirus
620 RNA cap guanine-N7-methyltransferase. *J Virol* **87**, 6296-6305, doi:10.1128/JVI.00061-13
621 (2013).

622 33 Ma, Y. *et al.* Structural basis and functional analysis of the SARS coronavirus nsp14-nsp10
623 complex. *Proc Natl Acad Sci U S A* **112**, 9436-9441, doi:10.1073/pnas.1508686112 (2015).

624 34 Agostini, M. L. *et al.* Coronavirus Susceptibility to the Antiviral Remdesivir (GS-5734) Is
625 Mediated by the Viral Polymerase and the Proofreading Exoribonuclease. *mBio* **9**,
626 doi:10.1128/mBio.00221-18 (2018).

627 35 Madelain, V. *et al.* Favipiravir Pharmacokinetics in Nonhuman Primates and Insights for Future
628 Efficacy Studies of Hemorrhagic Fever Viruses. *Antimicrob Agents Chemother* **61**,
629 doi:10.1128/AAC.01305-16 (2017).

630 36 Gowen, B. B. *et al.* Alterations in favipiravir (T-705) pharmacokinetics and biodistribution in a
631 hamster model of viral hemorrhagic fever. *Antiviral Res* **121**, 132-137,
632 doi:10.1016/j.antiviral.2015.07.003 (2015).

633 37 Madelain, V. *et al.* Ebola Virus Infection: Review of the Pharmacokinetic and Pharmacodynamic
634 Properties of Drugs Considered for Testing in Human Efficacy Trials. *Clin Pharmacokinet* **55**,
635 907-923, doi:10.1007/s40262-015-0364-1 (2016).

636 38 Madelain, V. *et al.* Modeling Favipiravir Antiviral Efficacy Against Emerging Viruses: From
637 Animal Studies to Clinical Trials. *CPT Pharmacometrics Syst Pharmacol* **9**, 258-271,
638 doi:10.1002/psp4.12510 (2020).

639 39 Sissoko, D. *et al.* Experimental Treatment with Favipiravir for Ebola Virus Disease (the JIKI Trial):
640 A Historically Controlled, Single-Arm Proof-of-Concept Trial in Guinea. *Plos Medicine* **13**,
641 doi:ARTN e1001967
642 10.1371/journal.pmed.1001967 (2016).

643 40 Ninove, L. *et al.* RNA and DNA bacteriophages as molecular diagnosis controls in clinical
644 virology: a comprehensive study of more than 45,000 routine PCR tests. *PLoS One* **6**, e16142,
645 doi:10.1371/journal.pone.0016142 (2011).

646 41 REED, L. J. & MUENCH, H. A SIMPLE METHOD OF ESTIMATING FIFTY PER CENT ENDPOINTS.
647 *American Journal of Epidemiology* **27**, 493-497 (1938).

648